JOURNAL OF AIRCRAFT
Vol. 36, No. 2, March–April 1999

Method for Accelerating the Destruction of Aircraft Wake Vortices

Steven C. Rennich* and Sanjiva K. Lele†
Stanford University, Stanford, California 94305-4035

The wake vortices shed by large aircraft and their associated hazard to following aircraft remain an important issue in commercial aviation. Extensive research into methods for alleviating this wake vortex hazard has been continuing for many years. This paper presents results from numerical simulations detailing a potentially useful mechanism for accelerating the destruction of the aircraft vortex wake and reducing the wake vortex hazard. The term *destruction* is used to refer to the progressive annihilation of the wake caused by mixing of vorticity of opposite sign and the associated elimination of large coherent structures. The emphasis here is on a description of the mechanism and its connection to previous work.

Introduction

ALL aircraft, as a consequence of producing lift, shed a vortex wake that typically evolves into a counter-rotating vortex pair. These vortices pose a danger to other aircraft. They each produce a region of strong rotational flow and, between them, a region of strong downwash. If a following aircraft encounters this wake at a shallow angle of incidence, it can experience a large upset in roll because of the rotating flow or a strong downwash, both of which can result in a significant loss of altitude. If this encounter happens when the aircraft is already near the ground, such as during takeoff or landing, the result can be disastrous. This vortex pair will eventually dissipate as a result of instabilities in the pair itself, atmospheric effects, or viscosity. However, in an unstratified, quiescent environment, the vortex pair can persist for very long times.[1,2]

To avoid this hazard, separation standards have been implemented that aircraft must observe when operating under instrument flight rules (IFR) conditions.[3] In almost all situations, if naturally occurring instabilities do not merge and destroy the vortices, these required separations allow sufficient time for the vortex pair to either convect itself out of the approach corridor or be blown out as a result of ambient winds. Unfortunately, these required separations also limit airport capacity. As air traffic increases without a significant increase in airport size or number, the wake vortex hazard poses a growing constraint. The potential introduction of very large commercial aircraft, with stronger, more dangerous wakes, will further aggravate this situation.

Background

In practice, the trailing vortices are often destroyed by the naturally occurring Crow instability.[4,5] In this instability, the counter-rotating vortex pair develops a symmetric, sinusoidal perturbation that lies in a plane inclined about 45 deg to the horizontal (plane containing the mean vortices). This perturbation grows until the vortices link and reconnect, forming a train of vortex loops. Figure 1 is a schematic that shows two wavelengths of this instability and defines the coordinate system used in this work.

Over the past 25 years, a large number of wake vortex alleviation methods have been investigated. Many of the initial efforts focused on either destroying the wake by mixing it with the surrounding irrotational fluid and, thus, reducing its intensity, or by exciting instabilities that would mix the vorticity of opposite sign. By contrast, many recent efforts have focused on methods for sensing the wake, predicting its development, and using that information to direct aircraft away from hazardous situations.[6–13] Despite the substantial amount of work performed, there is, as yet, no practical method for reducing this wake vortex hazard.

An earlier investigation of particular interest concerns the use of aircraft flaps as wake vortex attenuators.[14] In that work the primary focus was finding lift configurations that shed multiple vortices, which, upon merging, would have large, diffuse cores and pose a correspondingly reduced hazard. A particularly striking result is reproduced in Fig. 2. The photographs show a Boeing 747 with the inboard flaps extended to 30 deg and the outboard flaps extended to 1 deg. The edge vortices from the inboard flap are visualized with smoke generators located at the flap edges. Although significantly different from the instability in Fig. 1, a large sinusoidal undulation can be seen developing on the vortices shed from the inboard edge of the inboard flaps. Most importantly, pilots of Learjet and T-37B aircraft reported that at 3 n miles behind the 747 the wake posed no significant danger. This is compared with the 9 n mile separation requirement reported by the chase pilots when the flaps were deflected in the standard (30 deg/30 deg) landing configuration and to the 6 n mile IFR separation required by the Federal Aviation Administration (FAA) for small aircraft following heavy aircraft. Unfortunately, when the landing gear was extended, this phenomenon was not observed.

Approach

As many other researchers have, we approached this problem looking for methods by which the Crow instability could be excited at large amplitude early in the development of the wake.[15–22] The shed vorticity would inevitably form a counter-rotating vortex pair and the Crow mechanism is the most rapidly growing instability known to exist on such a system. Consequently, we began a numerical investigation into how perturbations, applied to the wake at the wing, would survive the roll-up process and excite the Crow instability in the resulting vortex pair. A thorough understanding of this process might suggest techniques for optimizing and accelerating it.

Presented as Paper 98-0667 at the AIAA 36th Aerospace Sciences Meeting, Reno, NV, Jan. 12–15, 1998; received April 6, 1998; revision received July 27, 1998; accepted for publication July 28, 1998.

*Graduate Research Assistant, Department of Aeronautics and Astronautics; currently Member of the Technical Staff, Massachusetts Institute of Technology, Lincoln Laboratory, 244 Wood Street, Lexington, MA 02420-9185. E-mail: srennich@ll.mit.edu. Member AIAA.

†Associate Professor, Department of Aeronautics and Astronautics and Mechanical Engineering, 359a Durand Buiding. E-mail: lele@leland.stanford.edu. Member AIAA.

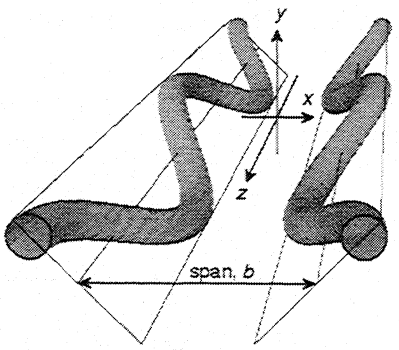

Fig. 1 Diagram showing two periods of the symmetric Crow instability.

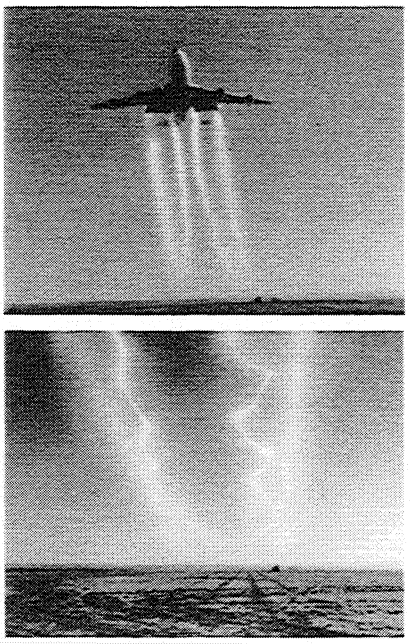

Fig. 2 Flow visualization photographs from flight tests of a Boeing 747 with flaps in a 30 deg/1 deg configuration and landing gear stowed.[14] The upper photograph shows the generating aircraft. The lower photograph shows the wake about 1 mile behind the aircraft. NASA Ames AC75-2671-2

Numerical Method

A new numerical method was developed specifically for this problem, which solves the incompressible Navier–Stokes (NS) equations in vorticity form in a domain that is unbounded in two directions and periodic in the third. The method uses a Fourier spectral representation in space and fourth-order Runge–Kutta time advancement (RK4). This code allows very detailed temporal studies of incompressible vortex wakes that exist in an unstratified atmosphere without any influence from the ground. The details of this method, as well as an assessment of its accuracy and efficiency, have been reported elsewhere.[23,24]

Because of the high cost of the NS simulations (the two NS computations presented next required about 12 h each on a Cray C90), a relatively simple vortex filament code has been used for low-cost parametric studies. This vortex filament code uses a single filament to represent each vortex, cubic splines to describe the filaments in space, the Biot–Savart law to compute the velocity, the cutoff method to desingularize the Biot–Savart equation, ghost vortices to enforce periodicity, and RK4 time advancement.[25–27] The validity of the vortex filament assumption is assessed (in the following text) through comparison to NS results. Its low cost (about 20 min on a personal computer) and success in reproducing trends makes the vortex filament code useful as an aid in guiding detailed NS simulations.

Previous Work

The new NS code was initially used for accurate simulations of the Crow instability occurring on a pair of counter-rotating vortices. Crow's inviscid, linear, vortex filament analysis was shown to predict the instability growth rates for the corresponding high Reynolds number, three-dimensional, viscous instability very well. The difference between the growth rate of the Crow instability in an inviscid fluid and that for a circulation-based Reynolds number of $\Gamma/\nu = 1 \times 10^4$ was on the order of 1%.[24] This suggests that the results from numerical simulations, performed at moderate Reynolds number, are relevant to the high Reynolds number ($\Gamma/\nu = 3 \times 10^7$) practical problem.

Another important previous result was the definition of measures useful in characterizing the size of perturbations on aircraft wakes. Two of these measures will be used in the present work. The first is termed the *displacement measure*. This is the maximum cross-plane displacement of the centroid of axial vorticity over the semispan, defined as

$$\delta_\Delta = \frac{1}{b_r\Gamma_r}\left(\left\{\int_A \left[\omega_z(z) - \omega_z\left(z + \frac{\lambda}{2}\right)\right] x\, dA\right\}^2 + \left\{\int_A \left[\omega_z(z) - \omega_z\left(z + \frac{\lambda}{2}\right)\right] y\, dA\right\}^2\right)^{1/2} \tag{1}$$

where λ is the wavelength of the fundamental (perturbation) mode, the dependence of axial vorticity, ω_z, on spanwise and vertical location, (x, y), is understood, the axial location, z, is chosen to maximize δ_Δ, and the integration is carried out over the half-plane containing only one semispan. (In some cases, the integration will be limited to a volume containing a single vortex.) Nondimensionalization is accomplished using appropriately chosen reference length and circulation scales, b_r and Γ_r, respectively.

The second measure that will be used is the *lift-based initial perturbation measure*, δ_L. This measure is formed from the amount of sloshing done to the lift distribution and is intended to represent the cost of imparting an oscillating perturbation to the wake:

$$\delta_L = \frac{1}{2b_r\Gamma_r}\int_{-(b/2)}^{b/2} |\Gamma'(x)|\, dx \tag{2}$$

Here, b is the span of the wing and Γ' is the oscillating perturbation to the spanwise lift distribution (harmonic in z with wavelength λ). Using this definition, δ_L is scaled such that for a rectangularly loaded wing with a small perturbation in span and root circulation (arranged to hold total lift constant) the two measures are initially equal. Thus, computed perturbation growth histories, initialized by a sloshing of size δ_L, can be compared with the predicted growth of the Crow instability with an initial amplitude of $\delta_\Delta = \delta_L$.

Description of Mechanism

Some exploratory NS simulations of the evolution of perturbations on a wake containing four vortices (with vortices from the same semispan having the same sign) had shown that as the weaker outer (tip) vortices were convected between the stronger inner (outboard flap edge) vortices, a region of high strain, the amplification of the perturbation was enhanced. However, as the tip vortices exited this region, the amplification reversed and there was little net enhancement. This in itself was interesting, but it also suggested that a vortex system that would not only place a vortex pair in a region of high strain, but would also keep them there, might sustain this enhanced growth. The construction of such a vortex system is not difficult.

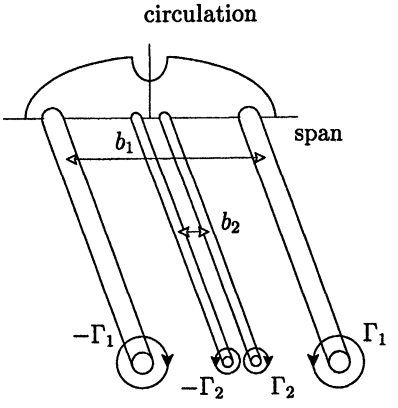

Fig. 3 Representative lift distribution and the associated system of shed vortices.

The simplest four-vortex system that achieves this result is diagramed in Fig. 3. Here, the inboard vortices are of opposite sign relative to the outboard vortices and convect themselves up, against the downwash induced by the outboard vortices. Such a system can be constructed such that it translates itself downward rigidly; i.e., such that the vortices do not evolve with respect to each other. In this way the inboard vortices can be kept in a region of high strain.

Mean Lift Distribution

The lift distribution shown in Fig. 3 is modeled as the superposition of two elliptical distributions. The larger distribution represents the basic lift across the wing and, the second, smaller distribution of opposite sign can be thought of as representing a loss of lift across the fuselage and between the high-lift devices. This is, of course, a very rough approximation to the lift distribution across an actual wing—it accounts for the inboard flap-edge vortices individually, but represents the outboard flap edge and tip vortices with a single vortex. However, it does capture the physics of the mechanism we are describing and, by limiting the number of shed vortices, simplifies its description.

In this system the larger outboard vortices have circulation Γ_1 and effective span b_1. The smaller inboard vortices of opposite sign have circulation Γ_2 and effective span b_2. The system is nondimensionalized using the span of the outboard vortices and the outboard circulation, resulting in the dimensionless span ratio:

$$\mathcal{X} = b_2/b_1 \tag{3}$$

and the dimensionless circulation ratio:

$$\mathcal{G} = \Gamma_2/\Gamma_1 \tag{4}$$

In the results that follow, the outboard circulation and span have been used to nondimensionalize Eqs. (1) and (2) as well ($\Gamma_r = \Gamma_1$, $b_r = b_1$).

A point vortex analysis can easily be used to determine the relative strengths and separations required to achieve a rigidly translating mean system. The result is

$$\mathcal{X}^3 + 3\mathcal{G}\mathcal{X}^2 + 3\mathcal{X} + \mathcal{G} = 0 \tag{5}$$

A *rough* survey of existing large aircraft shows that the separation between the inboard flap edges is about 10–15% of the span and, in the high-lift configuration, that there is approximately a 40–50% loss of lift across the fuselage. Figure 4 plots the solutions to Eq. (5) and shows the approximate space occupied by current aircraft.

Perturbation

This system is perturbed by giving b_1 and b_2 a small oscillation. The root circulations, Γ_1 and Γ_2, are left unchanged.

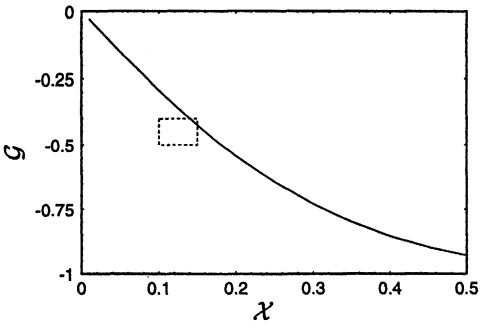

Fig. 4 Relationship between the circulation ratio, $\mathcal{G}$, and the span ratio, $\mathcal{X}$, such that the double vortex pair translates rigidly. The dashed box shows the region occupied by current aircraft.

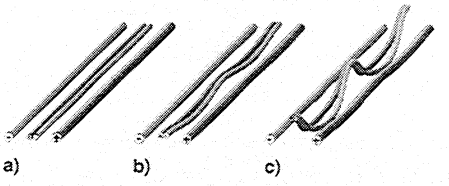

Fig. 5 Vortex filament simulation showing the perturbation amplification mechanism. Shading and end symbols denote vorticity of opposite sign: a) the four initial vortices each with an imperceptible perturbation, b) a Crow-type instability grows on the inboard vortices, and c) the perturbation to the inboard vortices continues to grow and begins to induce a perturbation on the outboard vortices.

The total lift is held constant by correctly sizing the perturbations and keeping them 180-deg out of phase. That is, as the outboard span, b_1, is reduced by a length δb and loses lift, the inboard span, b_2, falls by an amount $(-\mathcal{G})\delta b$, and exactly compensates for the lost lift.

Amplification Mechanism

The amplification of the perturbation begins in a way that is analogous to the Crow instability on a counter-rotating vortex pair. The portion of the inboard vortex pair that has been perturbed closer together will propagate upward (in a reference frame translating with the mean vortices) overcoming the downwash induced by the outboard vortices. The portion of the inboard pair that is perturbed farther apart will get convected downward. As the perturbation grows, the self-induced rotation of the inboard vortex will enhance this effect. The upwardly convecting portion will be rotated into a region of more rapidly moving upward flow, and the downwardly convection portion will be rotated into a region of more rapidly moving downward flow. Thus, the perturbation on the inboard vortices will experience very rapid growth.

The second, more important stage of the instability begins as the rapidly growing perturbation on the inboard vortices induces a large, Crow-type perturbation, i.e., one that contains a significant component of the pure Crow mode shown in Fig. 1, on the outboard vortices. It is this perturbation and subsequent destruction of the outboard vortices that is most important, and a Crow-type perturbation is desired because it will ultimately lead to the annihilation of vorticity through mixing of vorticity of opposite sign. This process is visualized, using results from a vortex filament calculation, in Fig. 5.

Vortex Filament Results

Because this instability is growing so rapidly, strong gradients in the axial direction develop quickly and make NS simulations very expensive. As a result of this, vortex filament methods have been used for initial studies. While only approximately correct in a quantitative sense, these simulations capture the dominant effects of the vortex dynamics and are a

useful tool for exploration. For these simulations the circulation ratio was held constant at $\mathcal{G} = -0.4$ and the vortex cores were sized according to the estimates of Spreiter and Sacks.[28] The axial perturbation wavelength was set to the most unstable wavelength predicted from Crow's analysis,[5] found using the effective span of the entire system. Because $\mathcal{G} = -0.4$ for all of the simulations presented in this paper, the effective span and, hence, the most unstable Crow wavelength for the entire vortex system, is the same. Again, using the estimates of Spreiter and Sacks, this perturbation wavelength, λ, is $8.53b_0$, where b_0 is the effective span.

Vortex filament simulations were used to investigate the behavior of this perturbation growth mechanism in cases when $\mathcal{X}$ and $\mathcal{G}$ did not satisfy Eq. (5). Figure 6a shows the late time development of a vortex filament calculation with $\mathcal{G} = -0.40$ and $\mathcal{X} = 0.125$ ($\mathcal{X}$ is too small). In this case, the inboard vortices are placed too closely together and they tend to eject themselves from the system. Although the inboard vortices still experience very large deformations, they do not impart a significant perturbation to the outboard vortices. Figure 6b shows the result when $\mathcal{X} = 0.155$ ($\mathcal{X}$ is too large). Here, the inboard vortices are too distant to counter the downwash induced by the two outboard vortices, and they get convected down and around the flap vortices. Notice, however, that a significant perturbation has emerged on the outboard vortices in this case.

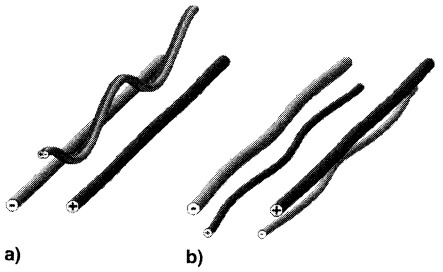

Fig. 6 Visualization of a) the inboard vortex pair being ejected from the system with $\mathcal{G} = -0.40$ and $\mathcal{X} = 0.125$, and b) the inboard vortex pair being completely entrained with $\mathcal{G} = -0.40$ and $\mathcal{X} = 0.155$. Shading and end symbols denote vorticity of opposite sign.

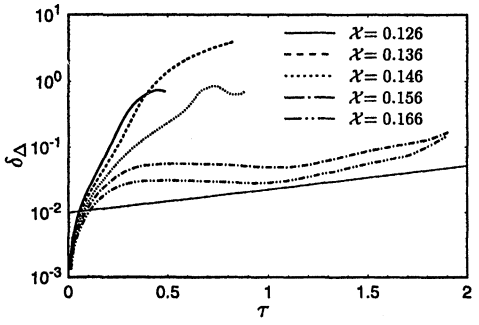

Fig. 7 Growth of the maximum displacement in the centroid of vorticity as a function of span ratio. The straight line shows the growth of the most unstable Crow mode occurring on the outboard vortices only. $\mathcal{G} = -0.4$.

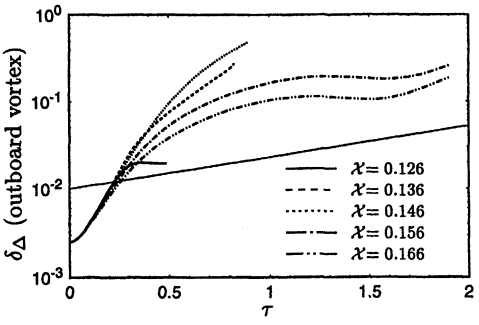

Fig. 8 Growth of the maximum displacement in the centroid of vorticity on the outboard vortex as a function of span ratio. The straight line shows the predicted growth of the most unstable Crow mode occurring on the outboard vortices only. $\mathcal{G} = -0.4$.

Figure 7 plots the growth of the perturbation for several values of $\mathcal{X}$. Again, $\mathcal{G} = -0.4$. The time, τ, has been nondimensionalized by $\Gamma_1/2\pi b_1^2$, the time required for the outboard vortices to translate downward a distance equal to their span. All simulations were given initial perturbations of size $\delta_L = 0.01$, a number thought sufficiently small to be realistic in a practical sense. Because, by construction, the initial perturbation to the centroid of vorticity is zero, the initial perturbation growth is very rapid. Notice, however, that smaller values of $\mathcal{X}$ display this rapid growth for longer periods. In fact, the growth rate appears to increase monotonically with decreasing $\mathcal{X}$. This result is misleading. As seen in Fig. 6a, this effect is caused by the rapid growth of the perturbation on the inboard vortices alone. In all cases, the simulation is terminated, either because of loss of resolution or the close approach of two vortices, a situation that this simple vortex filament method cannot model correctly. For comparison, the growth of the most unstable Crow mode occurring on the outboard vortices only ($\lambda = 8.53b_1$) is also shown.

Figure 8 shows the growth of the perturbation on the outboard vortices alone. In this case Eq. (1) is integrated over a volume containing only an outboard vortex. Again, the initial growth rate for all values of $\mathcal{X}$ is very rapid, but at later times the trend is no longer monotonic, and the most rapid growth corresponds to a value of $\mathcal{X}$ very near to that obtained from Eq. (5). The growth of the most unstable Crow mode on the outboard vortices is again shown for comparison. Figures 7 and 8 both show that the perturbation amplification achieved by this mechanism is much greater than that caused by the single-pair Crow instability.

NS Results

Two NS simulations have been performed that support the vortex filament results. These simulations are more realistic because they account for the shed spanwise vorticity and the roll-up process, and they can be run for longer times because the dynamics occurring when two vortices approach each other are accurately represented. They have been performed at a Reynolds number of $\Gamma_1/\nu = 1 \times 10^4$ and with span ratios of $\mathcal{X} = 0.161$ and 0.151. In both cases, $\mathcal{G} = -0.4$, the perturbation wavelength is $\lambda = 8.53b_0$, and the initial perturbation is sized by $\delta_L = 0.01$.

$\mathcal{X} = 0.161$

For computational reasons, the span ratio $\mathcal{X} = 0.161$ was chosen instead of the more rapidly growing $\mathcal{X} \approx 0.145$. A number of short simulations with varying span ratios showed $\mathcal{X} = 0.161$ to be the span ratio for which the closely perturbed portions of the inboard vortices would maintain a constant separation. The advantage in this was that the sharp gradients caused by the close approach and potential merging of the inboard vortices would not have to be resolved. Thus, this choice of span ratio would require fewer computational resources while still displaying the rapid amplification mechanism. The initial mesh was $256 \times 256 \times 24$ points and spanned a domain of size $(1.68 \times 1.68 \times 13.31)b_1$. Several times the vorticity field was interpolated to a larger domain to contain the growing perturbation. The final mesh was $176 \times 176 \times 128$ points and spanned a domain of size $(4.11 \times 4.11 \times 13.31)b_1$.[24]

Figure 9 gives a two-dimensional representation of the initial roll-up of the mean axial vorticity. The time, τ, is nondimensionalized as before, and the vorticity is made nondimensional using $2\pi b_1^2/\Gamma_1$. The familiar roll-up spirals are present. By time $\tau = 0.2458$, four distinct vortices have formed, with the inboard pair having descended below the outboard pair.

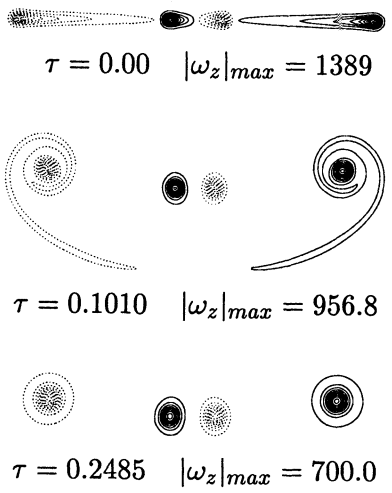

Fig. 9 Contours of mean axial vorticity showing the initial roll-up for the $\mathcal{X}$ = 0.161 case. Contours are spaced by 10% of the maximum vorticity magnitude. Solid and dotted lines denote vorticity of opposite sign.

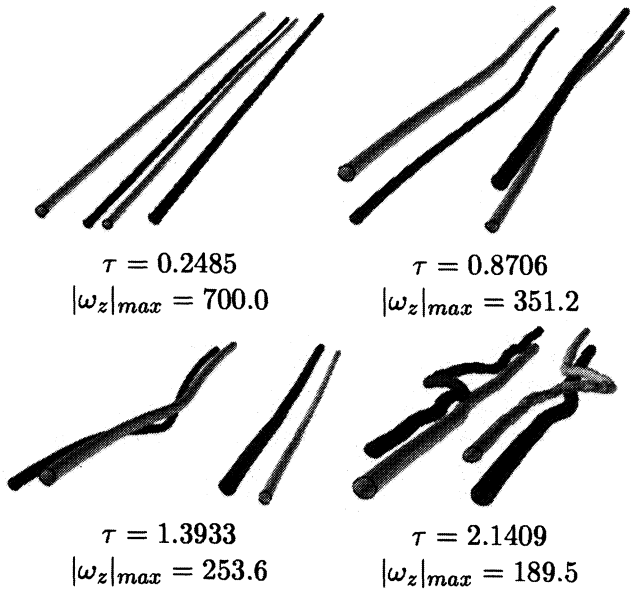

Fig. 10 Isosurfaces of axial vorticity for the $\mathcal{X}$ = 0.161 case. Contours are at 20% of the maximum vorticity magnitude. Differential shading denotes vorticity of opposite sign.

The late time development is shown by the three-dimensional visualizations in Fig. 10. This figure shows how the inboard vortices get convected down and around the outboard vortices. Although the initial perturbation contains only a single axial mode, by the last view there is a highly localized perturbation on the inboard and outboard vortices.

$\mathcal{X}$ = 0.151

The simulation with $\mathcal{X}$ = 0.161 was clearly free of any vortex reconnection, and so a second simulation with $\mathcal{X}$ = 0.151 was performed. Again, the domain was resized several times during the run. The initial mesh was 256 × 256 × 64 points and spanned a domain of size (1.69 × 1.69 × 13.36)b_1. The final mesh was 192 × 192 × 256 points and spanned a domain of size (2.82 × 2.82 × 13.36)b_1.[24]

Figure 11 presents a two-dimensional visualization of the roll-up of the mean axial vorticity. Again, the wake quickly develops into a double pair of counter-rotating vortices. During the roll-up process, the inboard vortices fall below the outboard vortices. However, unlike the previous case, at time τ = 0.2489, the mean inboard vortices are very nearly aligned with the outboard vortices. This suggests that $\mathcal{X}$ = 0.151 is quite close to the value required for the rigid translation of the mean vortices.

Figure 12 shows the subsequent three-dimensional evolution of the vortices. The first two visualizations are isosurfaces of axial vorticity magnitude with contours at 20% of the maximum. This simulation is displaying exactly the mechanism of interest. The resemblance to the vortex filament results shown in Fig. 5 is very good. As the vortex tubes become more distorted, axial vorticity alone ceases to give a good picture of the flow, and so the last two visualizations in Fig. 12 are of total vorticity magnitude. At τ = 1.1243, the contour level is at 5% to show the faint connection that still exists on the inboard vortices. At τ = 1.3273, the contour level has been set at 15% of the maximum to more clearly show the reconnection

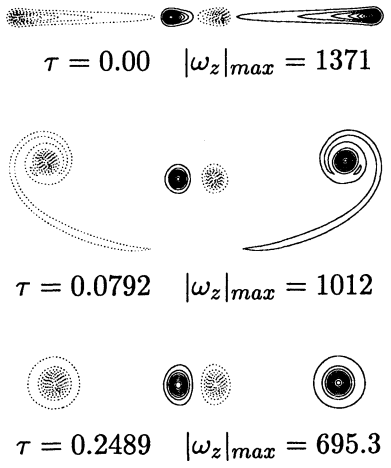

Fig. 11 Contours of mean axial vorticity showing the initial roll-up with $\mathcal{X}$ = 0.151. Contours are spaced by 10% of the maximum vorticity magnitude. Solid and dotted lines denote vorticity of opposite sign.

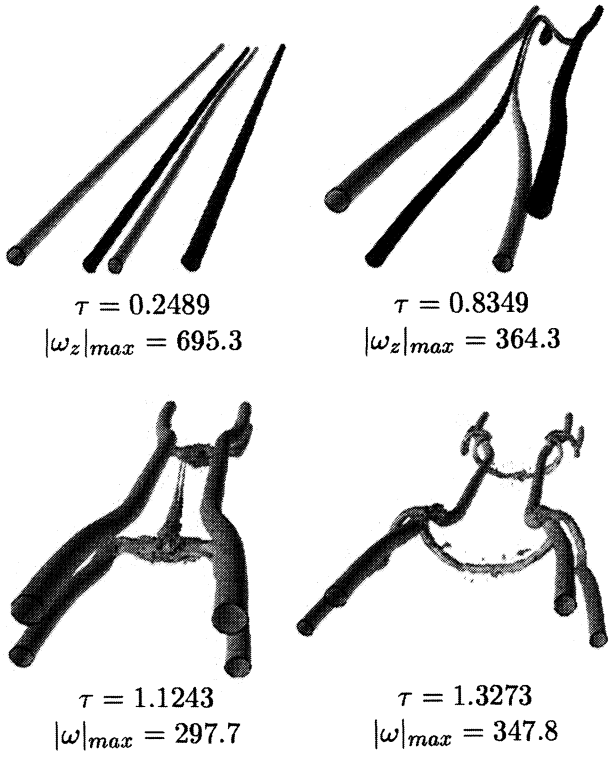

Fig. 12 Isosurfaces of axial vorticity/vorticity magnitude for the accelerated destruction scheme with $\mathcal{X}$ = 0.151. For times τ = 0 and 0.8349 contours are at 20% of the maximum axial vorticity magnitude.

that has taken place on the inboard vortices and how they are getting wrapped around the outboard vortices. Clearly, by time $\tau = 1.3273$, a very large Crow-type perturbation has developed on the outboard vortices.

Perturbation Growth

Qualitatively, the growth of the perturbations in the NS and the vortex filament cases compare well. All of the features present in Figs. 5 and 6 have been reproduced. The growth histories are quantitatively shown in Figs. 13 and 14. Figure 13 shows the growth of the displacement measure vs time for the two NS cases along with the $\mathcal{K} = 0.146$ vortex filament case and most unstable Crow mode for comparison. The initial growth rates for the NS and filament studies are similar, whereas at later times, the filament displays more rapid growth. By comparing with Fig. 7 it can be seen that the trends with respect to $\mathcal{K}$ are captured as well. For larger values of $\mathcal{K}$ the growth rate is reduced and becomes nonmonotonic. Most remarkably, at later times, the NS case with $\mathcal{K} = 0.151$ displays constant exponential growth with a rate that is very nearly equal to the growth rate for the most unstable Crow mode on the outboard vortex pair.

Figure 14 shows the displacement measure, applied to an outboard vortex alone, for the same three cases along with the most unstable Crow mode. When quantified in this way the NS and vortex filament cases are much less distinct. They all show much more rapid perturbation growth than the Crow mode. Note that the discontinuities and initial noise in the NS data result from remeshing the field to a larger domain and our method of separating the vorticity between the inboard and outboard vortices.

Discussion

Figure 15 shows isosurfaces of axial vorticity for three wavelengths of the $\mathcal{K} = 0.151$ NS simulation at $\tau = 0.65$. The viewpoint for this figure corresponds to an observer looking up at an aircraft passing overhead. These similarities between

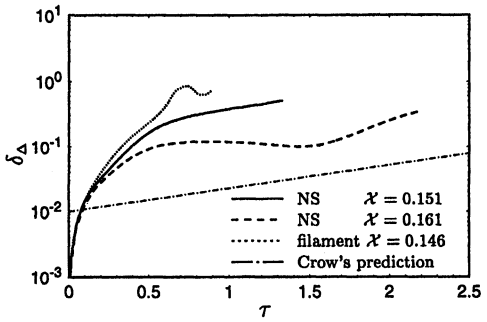

Fig. 13 Growth of the displacement measure, δ_Δ, for the two NS cases. The maximum Crow growth and a vortex filament result are included for comparison.

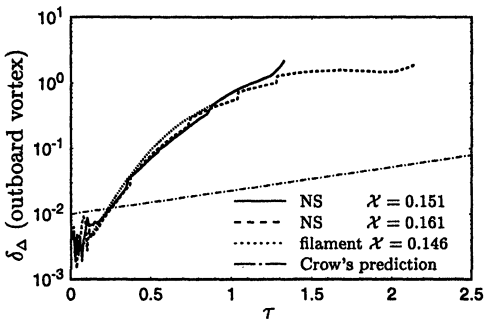

Fig. 14 Growth of the displacement measure, δ_Δ, computed over the outboard vortex only, for the two NS cases. The maximum Crow growth and a vortex filament result are included for comparison.

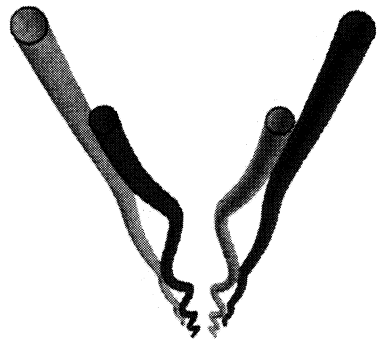

Fig. 15 Isosurfaces of axial vorticity, at 20% of the maximum, for three wavelengths of the $\mathcal{K} = 0.151$ NS simulation at $\tau = 0.65$.

Fig. 15 and the lower photograph in Fig. 2 suggest that it is exactly the mechanism described here that was taking place in the flight tests. The fact that pilots in chase aircraft reported a safe wake only 3 n miles behind the B-747, indicates that this is an effective method for alleviating the wake vortex hazard.

Two other intriguing observations can be made concerning the flight tests. First, the instability was not deliberately forced. This suggests that, even on calm days, ambient atmospheric turbulence may provide sufficient perturbation for significant hazard alleviation. Second, very effective alleviation was achieved with what is certainly a suboptimal configuration. Because the inboard vortices, as a whole, were convected downward, the span ratio in the flight test was too large. It is likely that even greater hazard alleviation could have been achieved by reducing the effective span ratio.

The upset of the alleviation mechanism by the extended landing gear emphasizes the fact that the entire vorticity field shed by the aircraft must be accounted for when designing such a wake vortex alleviation mechanism. That is to say, by including the vorticity shed by the landing gear in the analysis, a span ratio could be computed for the B-747 which would permit the alleviation mechanism to work in the presence of the landing gear.

The many possibilities for further optimizing this mechanism, and its application to systems containing more realistic distributions of vorticity, have yet to be investigated in detail.

Summary

In this paper a mechanism has been described that is potentially very useful in achieving alleviation of the aircraft wake vortex hazard. By configuring the inboard vortices such that they remain in a region of high strain, perturbations on these inboard vortices grow very rapidly. These highly perturbed inboard vortices then impart a large-amplitude Crow-type perturbation on the larger, more dangerous outboard vortices. The Crow mechanism will complete the destruction of the outboard vortices.

Both vortex filament methods and NS simulations have been used to investigate perturbation growth rates caused by this mechanism. Despite their many assumptions, the vortex filament methods have been shown to be at least qualitatively correct and a useful tool for initial investigations. The NS simulations, while expensive, have provided quantitative data regarding the perturbation growth rates. This new mechanism effectively increased the amplitude of the initial perturbation by an order of magnitude when compared with the most unstable Crow mode on a single vortex pair.

The connection between the method described here and the results of earlier flight tests is intriguing and further supports the existence and usefulness of this mechanism.

Acknowledgments

This work was supported by the National Science Foundation and the Boeing Commercial Airplane Company under the PYI award to Sanjiva K. Lele. We would also like to acknowl-

edge the Numerical Aerospace Simulation Facility for providing computational resources.

References

[1]Greene, G. C., "An Approximate Model of Vortex Decay in the Atmosphere," *Journal of Aircraft*, Vol. 23, No. 7, 1986, pp. 566–573.

[2]Spalart, P. R., and Wray, A. A., "Initiation of the Crow Instability by Atmospheric Turbulence," *The Characterisation & Modification of Wakes from Lifting Vehicles in Fluids*, AGARD, CP-584, 1996, 18-1–18-8 (Paper 18).

[3]Anon., *Federal Aviation Regulations—Airman's Information Manual*, A.S.A. Publications, Inc., Seattle, WA, 1987.

[4]Scorer, R. S., *Natural Aerodynamics*, Pergamon, New York, 1958.

[5]Crow, S. C., "Stability Theory for a Pair of Trailing Vortices," *AIAA Journal*, Vol. 8, No. 12, 1970, pp. 2172–2179.

[6]Olson, J. H., Goldburg, A., and Rogers, M. (eds.), *Aircraft Wake Turbulence and Its Detection*, Plenum, New York, 1971.

[7]Donaldson, C. duP., and Bilanin, A. J., "Vortex Wakes of Conventional Aircraft," AGARD, TR AG-204, May 1975.

[8]Widnall, S. E., "The Structure and Dynamics of Vortex Filaments," *Annual Review of Fluid Mechanics*, Vol. 7, 1975, pp. 141–165.

[9]Gessow, A. (ed.), *Wake Vortex Minimization*, NASA SP-409, NASA, Washington, DC, 1976.

[10]Hallock, J. N., "Aircraft Wake Vortices: An Assessment of the Current Situation," Volpe National Transportation Systems Center, DOT-FAA-RD-90-29, Cambridge, MA, Jan. 1991.

[11]Hallock, J. N. (ed.), *Proceedings of the Aircraft Wake Vortices Conference*, Volpe National Transportation Systems Center, DOT-VNTSC-FAA-92-7.1, Cambridge, MA, 1992.

[12]*The Characterisation & Modification of Wakes from Lifting Vehicles in Fluids*, AGARD, CP-584, 1996.

[13]Spalart, P. R., "Airplane Trailing Vortices," *Annual Review of Fluid Mechanics*, Vol. 30, 1998, pp. 107–138.

[14]Corsiglia, V. R., and Dunham, R. E., Jr., "Aircraft Wake-Vortex Minimization by Use of Flaps," *Wake Vortex Minimization*, NASA SP-409, 1976, pp. 305–338.

[15]Crow, S. C., "Panel Discussion," *Aircraft Wake Turbulence and Its Detection*, Plenum, New York, 1971, pp. 577–583.

[16]Bilanin, A. J., and Widnall, S. E., "Aircraft Wake Dissipation by Sinusoidal Instability and Vortex Breakdown," AIAA Paper 73-107, Jan. 1973.

[17]Chevalier, H., "Flight Test Studies of the Formation and Dissipation of Trailing Vortices," *Journal of Aircraft*, Vol. 10, No. 1, 1973, pp. 14–18.

[18]Crow, S. C., and Bate, E. R., Jr., "Lifespan of Trailing Vortices in a Turbulent Atmosphere," *Journal of Aircraft*, Vol. 13, No. 7, 1976, pp. 476–482.

[19]Barber, M. R., and Tymczyszyn, J. J., "Wake Vortex Attenuation Flight Tests: A Status Report," NASA CP-2170, 1980, pp. 387–408.

[20]Jordan, F. L., "Flow Visualization of the Wake of a Transport Aircraft Model with Lateral-Control Oscillations," NASA TR TM-84623, June 1983.

[21]Rossow, V. J., "Wake Hazard Alleviation Associated with Roll Oscillations of Wake-Generating Aircraft," *Journal of Aircraft*, Vol. 23, No. 6, 1986, pp. 484–491.

[22]Crouch, J. D., "Instability and Transient Growth for Two Trailing-Vortex Pairs," AIAA Paper 97-0062, Jan. 1997.

[23]Rennich, S. C., and Lele, S. K., "Numerical Method for Incompressible Vortical Flows with Two Unbounded Directions," *Journal of Computational Physics*, Vol. 137, No. 1, 1997, pp. 101–129.

[24]Rennich, S. C., "Accelerated Destruction of Aircraft Wake Vortices," Dept. of Aeronautics and Astronautics, TR SUDAAR 705, Stanford Univ., Stanford, CA, Sept. 1997.

[25]Leonard, A., "Vortex Methods for Flow Simulation," *Journal of Computational Physics*, Vol. 37, 1980, pp. 289–335.

[26]Leonard, A., "Computing Three-Dimensional Incompressible Flows with Vortex Elements," *Annual Review of Fluid Mechanics*, Vol. 17, 1985, pp. 523–559.

[27]Saffman, P. G., *Vortex Dynamics*, Cambridge Univ. Press, Cambridge, England, UK, 1992.

[28]Spreiter, J. R., and Sacks, A. H., "The Rolling Up of the Trailing Vortex Sheet and Its Effect on the Downwash Behind Wings," *Journal of the Aeronautical Sciences*, Vol. 18, No. 1, 1951, pp. 21–32.